# Breast Lesions Segmentation in Dynamic Contrast-Enhanced MR Images

Hamza Bouchefra
Biomedical Image Sciences
University Utrecht

## Abstract

Breast cancer is a serious public health problem worldwide. An accurate segmentation of the breast lesion is important for clinical applications in monitoring tumor volume and in the quantification of tumor characteristics. Dynamic contrast-enhanced magnetic resonance imaging can be used in accurate segmentation and quantification of breast lesions. The aim of this review is to provide an overview of the methods of breast lesion segmentation methods in Dynamic Contrast-Enhanced MR Images. In this study, semi-automatic and automatic methods are reviewed. The algorithms that are employed in these articles are fuzzy c-means, neural networks, marker-controlled watershed, active contour model, Markov random field, connected component analysis, graph cut, region growing and level set. The fuzzy c-means clustering algorithm is a popular method used by most of the articles. A limitation of many studies is the small number of datasets. Although the datasets were not the same throughout the articles, the method used in Pang et al. [7] outperforms the other methods that showed both good and robust results and is potential for further research.

## I. Introduction

A breast lesion is an abnormal tissue in the breast that has the risk to be cancerous. Breast cancer is the most common cancer and a leading cause of deaths in females worldwide. However, early detection of breast lesions can increase the chance of successful treatment.

Segmentation is the process of dividing an image into regions with similar properties such as voxel intensity, color, texture, brightness and contrast. It is important to have a good segmentation of the breast lesion in scans because of the better quantification of tumor characteristics, the better localization in the radiotherapy treatment, and the better monitoring of response to therapy in follow-up sessions.

Segmentation can be done manually by experts, but this is a labor-intensive task and it is subject to intra- and inter-observer variability. This variability is highly present in cases where both the lesion and the breast tissue would appear white, particularly in dense breast tissue. Therefore, automatic segmentation methods are desired.

Automatic segmentation of breast lesion makes the process more robust and accurate. However, this is a challenging task since the lesions may have complicated topological structures, and intensity distributions that are similar to the surrounding tissue. Also the presence of other structures that resemble lesions e.g. lymph nodes, parts of blood vessel, may complicate the segmentation process.

X-ray mammography is currently regarded as the standard diagnostic tool for breast cancer. The main disadvantage of this method is the possibility of missing the lesion in case of dense-breast tissue [1, 2]. Dynamic contrast-enhanced MR imaging (DCE-MRI) [3] offers superior contrast and high quality images compared to X-ray imaging. Therefore, DCE-MRI provides more information on the medical images, and makes it easier to distinguish the lesion from the background. Boetes et al. [4], Esserman et al. [5] and Malur et al. [6] have compared DCE-MRI against other imaging modalities and demonstrated that DCE-MRI is superior in determining breast cancer tumor volume.

In this paper, firstly we provide several methods that segment breast lesions on DCE-MRI images in section II. In section III, we review the explained methods, and then we conclude the paper.

## II. Methods

In this section, we discuss the different types of methods for the segmentation of breast lesions. Segmentation methods can be placed in three categories: manual, semi-automatic and automatic segmentation methods. Semi-automatic methods require user interaction such as placing a seed point or drawing a rectangle around the lesion whereas automatic methods do not require any interaction during the segmentation process.

*Segmentation based on the marker-controlled watershed*

The watershed transform is formally defined in terms of flooding simulations but can also be used for image segmentation. By seeing an image as a surface and take the bright areas as “high” and the dark areas as “low” surface, the line that causes the separation is called the watershed line and simplifies the segmentation. This works even better when marking foreground objects and background locations.

In Cui et al. [7], first a human operator draws an ellipse-shaped region of interest (ROI) that includes the entire tumor in a user interface. Because this study includes dynamic data, the ROI on one slice may not cover the tumor on another slice. Therefore for the initial delineation of the ROI, a slice was chosen where the tumor appeared larger than on the other slices so it would cover the whole tumor on the other slices.

In order to use the marker-controlled watershed, two markers are needed that define a search space for the detection of the target boundary. The two markers are in fact incorporated in a binary mask. To achieve this binary mask a Gaussian mixture modeling is applied on the ROI. This gives us an upper threshold, $T_{upper}$, and a lower threshold, $T_{lower}$, that is used in the determination of the markers. With the dual thresholds two markers are derived. An internal marker which is the area inside the ROI whose pixel intensities are higher than $T_{upper}$ and an external marker which is the union of the whole region outside the ROI and the area inside the ROI whose pixel intensities are lower than $T_{lower}$.

Now the internal and external markers are determined a gradient image is taken from the smoothed original image with the Sobel operator. To prevent that local minima will occur elsewhere than in the regions of the markers the gradient image is modified with a grayscale reconstruction algorithm [8]. Finally the watershed transform is applied and a final contour is obtained between the markers, which completes the segmentation of the tumor.

Now that one slice is processed the slices that are left are processed by a propagation strategy [9]. The segmented tumor is first dilated with a round structure element, whose diameter was proportional to the spacing of the adjacent two slices, so that this dilated region is used in the next slice as the ROI. Together, the dual thresholds are also passed without any change. The same procedure is done here. The internal and external markers are determined based on the dual thresholds and the watershed transform was performed to segment the tumor in the current slice. This continues until no pixel in the ROI has an intensity greater than $T_{upper}$.

*Segmentation based on connected component analysis*

Connected component analysis is an algorithm that scans an image and groups its pixels into components that share similar pixel intensity values and are in some way connected with each other. Each pixel is labeled with a color according to the component it was assigned to.

The complete segmentation process in Meinel et al. [10] included four steps: interactive lesion selection, automatic intensity threshold estimation, connected component analysis and a post-processing procedure for hole-filling and leakage removal. Before any lesion selection can be done, the data acquired in this study has to be preprocessed due to using of different imaging protocols at different institutions. Preprocessing steps consist of re-sampling and de-noising of the images.

Two different approaches are used to select a lesion, first one necessitates the user placing a seed point into the enhancing portion of the lesion and the second approach is done by placing a circular ROI around the lesion.

Proceeding to the next step is the threshold estimation. According to the seed-point-based lesion selection 1D rays are casted along directional vectors starting at the seed-point position [Figure 1]. Samples of the image data are sampled along each ray produce a 1D signal per ray. What is expected beforehand is a plunge in the signal intensity at a boundary, in this case a lesion boundary due to the enhancement of the contrast, and therefore the local minima of the derivative of the 1D signal will consist of boundary candidates. Only one boundary candidate will be chosen which is the closest to the seed-point. This is repeated for every ray and each will yield one boundary candidate. In order to estimate the threshold, first the most likely outliers are removed from the set by taking 25% of the boundary candidates with the smallest and largest distance to the seed-point. Finally, the threshold value is the mean intensity of the remaining boundary candidates. This mean intensity is calculated by reordering the N candidate points in ascending distance from the seed-point and applying the following formula:

$$T = \frac{2}{N} \sum_{i=N/4}^{3N/4-1} I(b^{\sigma(i)})$$

where T is the threshold, N is the number of candidate points, I is the intensity, b is the boundary point and σ denotes the permutation used for reordering the $b^i$. The second approach of selecting a lesion is done by placing a circular ROI around the lesion. The user can do so by drawing a circle with the mouse pointer. For the determination of the seed-point position a strong linear diffusion to the ROI is applied and the brightest pixel is used as the seed position.

The third step is a raw segmentation of the breast lesion which contains errors that are fixed by post-processing. The raw segmentation is performed using the intensity threshold and apply connected component (6-connectivity) starting from the seed-point position. Every pixel that has an intensity greater or equal than the threshold is included in the initial segmentation result. The errors that arise here are "holes" and leakage into vessels which need to be corrected. The "holes" that originate from non-enhancing areas, due to necrosis for example, are filled and any leakage is removed from the raw segmentation which concludes the segmentation process.

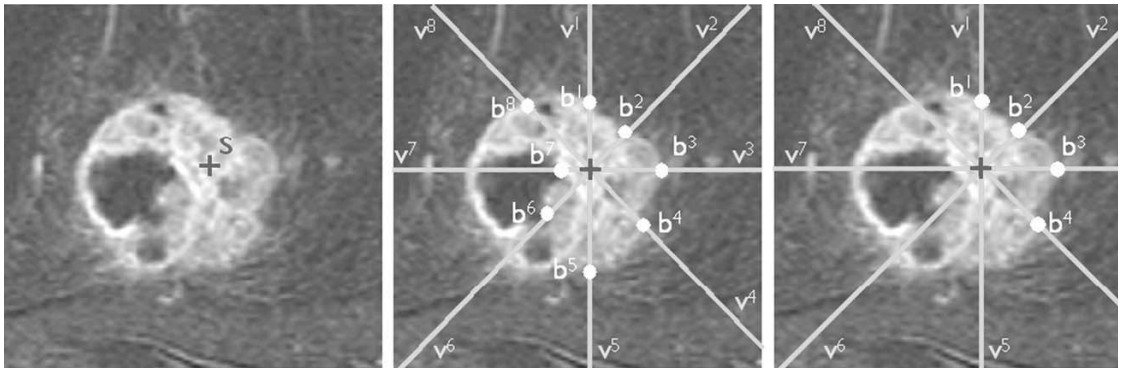


**Figure 1.** Seed-point selection along with casted rays along directional vectors starting at seed-point position

*Segmentation based on neural networks*

Unlike most segmentation methods, segmentation based on neural networks are trainable segmentation methods that can learn the distribution patterns of features of pre-known class specifications. Consisting of an input layer, a hidden layer and an output layer, each node in a layer receives input from all the nodes in the preceding layer.

The neural networks used in these papers each used a different number of input and output nodes, but both used the signal-time curve of each pixel as a feature for the classification. Each output node corresponds to a tissue class that the pixel is classified to. The output nodes results in a percentage giving the probability of the pixel belonging to a certain tissue class. This way each pixel is classified.

The microcirculation of tissue within malignant and benign lesions is different. This difference gives a variation in the MR signal over time what can be used for lesion detection. Several

techniques exist that are using this property to analyze these signal-time curves as can be seen in Gunnar et al. [11] and in June S et al. [12]. The use of neural networks over other classification techniques for the analysis of signal-time curves can bypass some restrictions of the techniques that are mentioned before. Segmenting breast lesions with neural networks is computationally faster and does not require a priori knowledge about the subject, what made it become a widely used technique. Since data are not the same everywhere or a different imaging sequence is used, the neural network has to be retrained with the different data sets.

In Lucht et al. [13] a multilayer perceptron (MLP) with 28 nodes in the input layer, 4 nodes in the hidden layer and 3 nodes in the output layer was used to classify the signal-time curves. The 3 nodes correspond to “carcinoma”, “benign lesion” and “parenchyma” that the lesion is classified with. The network analyzed the signal-time curve of each pixel and calculated the probability of that curve to which class it belongs. After the classification each pixel was superimposed in red or green determined by the classification it got. Pixels that were classified as “carcinoma” were superimposed in red, pixels that were classified as benign were superimposed in green and pixels classified as “parenchyma” were omitted. This way a segmentation can be made of the lesions by extracting the pixels that have the color red or green to further analyze the lesion in detail.

*Segmentation based on fuzzy c-means*

The fuzzy c-means (FCM) algorithm is an unsupervised learning technique that is widely used in different areas, frequently in pattern recognition. It is basically a method that clusters a piece of data to one or more clusters, meaning to divide a large data set into smaller data sets of some similarity.

As proposed in Chen et al. [14] the method consist of six steps for the lesion segmentation to complete. Firstly, to indicate the location of the lesion a box-shaped ROI containing the lesion is selected. This is done by drawing a rectangle around the lesion on the slice where this lesion appears at first, on the slice where this lesion appears as last and finally some middle slice where the rectangle is containing the lesion at his largest extent. The first and last slices define the cross-slice extent of the lesion. This ROI is duplicated on each slice and every time series.

Next, the ROI series are enhanced after the contrast has been delivered. This is done by dividing the post contrast intensity value of each voxel of every time series by the pre contrast intensity value of the same voxel. In other words, you will have an enhancement of every voxel for every time series.

In the following step the goal is to partition the voxels in the ROI into two clusters, either lesion or non lesion. In order to achieve that with the FCM algorithm, a partition matrix U and a prototype matrix V are needed. The prototype matrix V contains the class prototypes of the voxels and the partition matrix U contains the membership of the $i^{th}$ data point to the $k^{th}$ class of each voxel. The prototype matrix V is randomly initialized and the partition matrix U is found when minimizing the generalized least-squares error function $J_m$:

$$J_m = \sum_{k=1}^{c} \sum_{i=1}^{N} u_{ki}^{b} \|\mathbf{x}_i - \mathbf{v}_k\|^2$$

with the following constraint

$$\sum_{k=1}^{c} u_{ki} = 1,\ \forall\, i; 0 \le u_{ki} \le 1,\ \forall\, k, i; \sum_{i=1}^{N} u_{ki} > 0,\ \forall\, k$$

Where $b \in [1,\infty)$ is a weighting exponent on each fuzzy membership, and $\|\ \|$ denotes the Euclidean distance.

Both the matrix U and V are iteratively updated until convergence, meaning that the absolute change in consecutive iterations is less than $\epsilon = 10^{-5}$. Matrix U is updated with equation

$$u_{ki} = \frac{1}{\sum_{l=1}^{c} \left( \frac{\|\mathbf{x}_i - \mathbf{v}_k\|}{\|\mathbf{x}_i - \mathbf{v}_l\|} \right)^{2/(b-1)}}, \quad k = 1, 2, \ldots, c;\ i = 1, 2, \ldots, N$$

and matrix V with equation

$$v_k = \frac{\sum_{i=1}^{N} u_{ki}^b \mathbf{x}_i}{\sum_{i=1}^{N} u_{ki}^b}, k = 1, 2, \ldots, c$$

Because the enhancement in the lesion area is much more significant than elsewhere $U$ is the lesion membership map. This map is then binarized with a threshold of 0.2.

Due to vessels near the lesion or background noise there might be some false-positive voxels surrounding the lesion which must be reduced simply because they don't contribute to the segmentation of the lesion. This is done by a 3D connected-component labeling operation.

Because the lesion might have some necrotic area that did not enhance very much during the FCM procedure, this part will mistakenly be marked as a non lesion and will be visible as a hole in the 3D lesion. These holes are filled based on morphological reconstruction [34] which completes the segmentation

Kannan et al. [15] proposed a method that tries to minimize the objective function of FCM. This way, pixels whose intensities that are close to the center of its particular cluster will get a high membership value and pixels whose intensities are far from the center will get a low membership value. Based on this assumption the clustering of the objects become more reasonable. In the paper the breast is segmented by the new objective function, but with the same refined FCM lesions can be segmented as well.

In Shi et al. [16] the complete segmentation is done by an initial segmentation followed by a level set segmentation that is used to refine the initial segmentation. In both the segmentation methods, the FCM clustering is used. The initial segmentation, to obtain an initial segmentation volume, starts by assigning each data sample to all predefined clusters with respective likelihoods. The objective function used in this iterative process is a generalized least-squares error that is optimized during this process. The objective generalized least-squares error function

$$J = \sum_{i=1}^{N} \sum_{j=1}^{2} u_{ij}^2 \|\mathbf{x}_i - \mathbf{c}_j\|^2$$

with

$$u_{i1} + u_{i2} = 1, \quad \forall\, i = 1, \ldots, N$$

stopped when $J$ changed less or equal to 0.01 between two consecutive iterations or when 100 iterations were completed. In each iteration the $u_{i1}$ and $u_{i2}$ for every pixel in the 3D volume of interest (VOI) is updated by the following

$$u_{i1} = \frac{\|\mathbf{x}_i - \mathbf{c}_2\|^2}{\|\mathbf{x}_i - \mathbf{c}_1\|^2 + \|\mathbf{x}_i - \mathbf{c}_2\|^2} \quad \text{and} \quad u_{i2} = \frac{\|\mathbf{x}_i - \mathbf{c}_1\|^2}{\|\mathbf{x}_i - \mathbf{c}_1\|^2 + \|\mathbf{x}_i - \mathbf{c}_2\|^2}$$

Each pixel will have a likelihood $u_{i1}$ and $u_{i2}$. $u_{i1}$ indicating that how likely $v_i$ belongs to the background tissue and $u_{i2}$ telling how likely $v_i$ belongs to the malignant mass. To get a nice and clear view of the VOI which voxel belongs to the background tissue and which one to the malignant, the FCM clustering is binarized. This is done by assigning each voxel $v_i$ to the malignant mass if $u_{i2}$ was larger than a determined threshold $T$ of 0.3. Of this result, the largest 3D connected component is selected and the rest of the voxels were put in the background.

Breast masses on DCE-MR scans may demonstrate rim enhancement causing the segmented object containing holes. These are formed by groups of voxels that were assigned to the background tissue and surrounded by voxels that were assigned to the malignant mass. A morphological filling operation is used to fill these holes followed by a morphological opening operation. This completes the initial mass segmentation.

The 3D level set method refines the initial segmentation. The FCM clustering result is used in the 3D level set (LS) method as an extra external force for the regulation of the LS evolution. The rest of the LS formulation used is common to that in the literature [17-19]. The new included external force $u_2(x, y, z)$ is the FCM membership function that quantitatively defines the likelihood that a voxel belongs to a mass. This membership $u_2$ is based on the voxel intensity of the most enhanced VOI and also includes the dynamic enhancement information. The partial differential equation used is formulated as

$$\frac{\partial \varphi}{\partial t} + (|\vec{V}_0| - b\kappa + \alpha u_2)|\nabla \varphi| + \vec{G} \nabla\, \varphi = 0$$

where $|\vec{V}_0| = 1/1 + |\vec{G}|$ and $b = 2|\vec{V}_0|$. The free parameter $\alpha$ regulates the external force $u_2$

This formula contains the information that the LS should move fast on a flat surface and evolve slowly when nearing object edges.

In Pang et al. [20] an experienced radiologist identifies suspicious areas of breast lesions by a rectangle region of interest. These rectangle regions interest serve as an input in the two-step segmentation method, segmentation by fuzzy c-means and snake algorithm, to find the exact

contour of the lesions. The first segmentation method produces an initial segmentation of the ROI. This initial segmentation is then refined by the gradient vector flow (GVF) snake method.

Since the breast contains soft and different tissues, the MR images have overlapping intensities. This is because of the noise and blur in the acquisition what makes it hard to distinguish borders in the MR image. Also, if the resolution of a scanner is not high enough it may contribute an additional problem of blurred borders in the MR image. This is because resolution can be thought of as the ability to depict two distinct events in spatial resolution. Therefore, the higher the resolution of the medical imaging system the lower the blurring.

The advantage of the FCM clustering method in this case is that it allows voxels belong to different clusters with a certain likelihood. The final initial segmentation contains a binarized image that is formed by binarizing the membership map with a likelihood threshold of 0.5. This binarized image is then morphologically filled, morphologically opened and applied 2D connected-component labeling. This results in a segmentation that is slightly reduced in size.

Next, the refinement of the initial segmentation starts by applying the GVF snake model. In this segmentation method, a curve is tried to fit to the contour of the lesion that is driven by two forces. An “internal force” and an “external force” are forcing the curve its way to the contour. Such a curve can capture the irregular shapes and shape deformations that are known in lesions.

The external field is the vector field $\mathbf{v}(x, y)$ that is defined as $(u(x, y), v(x, y))$. This external field minimizes the energy functional

$$\varepsilon = \iint \mu\left(u_x^2 + u_y^2 + v_x^2 + v_y^2\right) + |\nabla f|^2 |\mathbf{v} - \nabla f|^2 \, dxdy$$

where $\mu$ is a regularization parameter. The parameter curve is defined as $\mathbf{x}(s) = (x(s), y(s))$ where $s$ denotes an arc length parameter. The segmentation of the GVF is done when a balance is reached between the internal force and the external force. The internal force is defined as $\alpha\mathbf{x}''(s) - \beta\mathbf{x}''''(s)$. The function of the internal force is to prevent the curve from stretching and bending excessive, where at the same time the external force is pulling the curve toward the contour of the lesion. In some situations it can be hard to reach a balance due to a too blurry or complex image. In that case a maximum number of iterations is set.

*Segmentation based on Markov Random Field model*

The Markov Random Field (MRF) model is a statistical model that can be used in segmentation methods. Despite of its widely usage in medical image segmentation it has two critical weaknesses. Its computational complexity and sensitivity of the result to the models parameters.

In Azmi et al. [21] they overcome these weaknesses by presenting an Improved-Markov Random Field (I-MRF) method. The purpose of MRF is to assign a pixel to a class in which the neighbors pixels are assigned to. This makes this method not a segmentation method in itself but more a statistical model. This method is therefore used in combination with the Finite Gaussian

Mixture (FGM). The FGM is mathematically a simple model and the computation of it can be done efficiently. Not only the computation efficiency makes it attractive but also the fact that MRF overcomes the limitation of FGM of not considering spatial information. FGM only uses the intensity histogram for segmentation what makes it sensitive to noise and other artifacts.

MRF has in fact a much larger computation overhead that the FGM due to the use of an iterative optimization methods to find appropriate distribution of labels, but its results are better. In I-MRF the need of an iterative method is eliminated by applying the ratio of two conditional probability distributions to estimate the prior distribution. The main idea of the model is that a pixel is more likely to be of a certain tissue type if the neighboring pixels are also of the same type.

*Segmentation based on geodesic active contour*

Geodesic active contours are a novel scheme for the detection of object boundaries. It attempts to minimize an energy associated to the current contour as a sum of an internal and external energy.

In Shannon et al. [22], before they let any segmentation be done with this method, every radiologist-selected slice at each time point, pre- and post-contrast, where the lesion is visible, a three-dimensional matrix is compiled. This matrix is defined as the image scene as following,

$$\mathcal{C} = (C, f^t)$$

$C$ is a spatial grid of voxels and $f^t$ is the associated signal intensity at time point $t$. The task of the EM algorithm, that is run interactively, is then to group all voxels that are similar on their time-series coefficient matrix. This is done by computing the posterior probability for every voxel to a certain class. The classes in this article are 4 Gaussian mixtures that are chosen empirically. The Expectation step of the EM algorithm calculates the probability and the Maximization step recalculates or updates the model parameters. Eventually after the EM algorithm is calculated every voxel is assigned a class, that is the class with the highest probability in the Expectation step, resulting in an image with voxels that are assigned to one of the four classes.

This image is then used as an initialization in the Magnetostatic Active Contour (MAC) model [23] to segment the lesions. This segmentation is based on a force field F that is interacting between the contour and the boundary of the object where both are treated as a current carrying loop. For each image scene $C$ there will be $K$, in this case $K$=4, class likelihood scenes constructed $L_k = (C, \ell_k)$. Each likelihood scene is constructed as following:

In each likelihood scene we construct ($C$, $l_k$) where $l_k(c)=P(D_k|a_c)$ $\forall C$. The result of $L_k$ is a binarized scene. This is obtained by the following formula,

$$\ell_k^B(c) = \begin{cases} 1, & \text{if } \ell_k = \max_k [P(D_k|a_c)] \\ 0, & \text{otherwise.} \end{cases}$$

From the 4 binarized scenes one is manually selected by the user that will serve as the initialization of the active contour.

*Segmentation based on graph cut*

This article describes a segmentation method that is based on graph-cut. Every pixel with a similar temporal enhancement is assigned the same label. For the initialization of the algorithm the tumor has to be specified and roughly segmented. Since this method improves on a coarse manual segmentation and therefore an expert rater is not needed, this is done by a manual rater. A rectangle region is drawn around the segmented tumor that is specified as a domain for the segmentation and a classification of both the tumor and background into 3 classes. This classification into 3 classes is done using k-means clustering. The interim result is an image with 3 labels. The output of the k-means clustering is used as an initialization in the following energy function

$$\begin{aligned} E = & \sum_{i \in \Omega} E_1(l_i) \\ & + \lambda_1 \sum_{<i,j> \in \mathcal{N}} E_2(l_i, l_j) \\ & + \lambda_2 \sum_{<i,j> \in \mathcal{N}_d} E_3(l_i, l_j) \\ & + \lambda_3 \sum_{<i,j> \in \mathcal{N}_{tb}} E_4(l_i, l_j) \end{aligned}$$

that is minimized by the expansion move algorithm [24] where $l_i$ is the label of pixel $i$. Factors $\lambda_1$, $\lambda_2$, $\lambda_3$ are used to adjust the relative importance of the four terms, and are empirically set to 1, $\Omega$ represents the image. The terms $E_1$ ensures statistical similarity, $E_2$ penalizes different label assignment, $E_3$ introduces fidelity and $E_4$ attempts to find the tumor boundary in the vicinity of manually placed contour. When the expansion move algorithm converges, the enhanced tumor region is the union of all tumor classes that is found by the algorithm.

| Article | Segmentation method | (Semi-) automatic | # patients/ breast DCE-MRI studies | Mean Volume overlap ratio (%) | Mean Area under the curve ($A_z$) | Mean Boundary distance (pixels) | Sensitivity (%) | Specificity (%) | t-test *p* value | Correlation coefficient (%) |
|---|---|---|---|---|---|---|---|---|---|---|
| Cui et al.[30] | Marker-controlled watershed | Semi-automatic | 13 | 62.6 ± 9.1 [a] | N/A | N/A | N/A | N/A | 0.0104 [a] | 0.6809 [a] |
| Shannon et al.[24] | Geodesic Active Contour | Automatic | 41 | N/A | N/A | N/A | 73 e<br>82 f<br>47 g | 99 e<br>99 e<br>99 e | N/A | N/A |
| Woods et al.[28] | Neural Network | Automatic | 4 | N/A | 0.99948 [a] | N/A | N/A | N/A | N/A | N/A |
| Schlossbauer et al. [29] | Region growing | Semi-automatic | 82 | N/A | N/A | N/A | N/A | N/A | N/A | N/A |
| Zheng et al.[27] [a] | Graph-Cut | Automatic | 31 | N/A | 0.97 | 4.10 ± 5.62 | N/A | N/A | N/A | N/A |
| Chen et al.[34] [a] | FCM | Automatic | 121 | 64.0 ± 12.0 | N/A | N/A | N/A | N/A | 0.71 [a] | 0.98 [a] |
| Szabó et al.[21] | Neural Network | Automatic | 10 | N/A | N/A | N/A | N/A | N/A | N/A | N/A |
| Lucht et al.[14] | Neural Network | Automatic | 15 | N/A | N/A | N/A | N/A | N/A | N/A | N/A |
| Kannan et al.[15] | FCM | Automatic | unknown [h] | N/A | N/A | N/A | N/A | N/A | N/A | N/A |
| Azmi et al.[22] | New MRF | Semi-automatic | 5 | 73.31 ± 9.36 | 0.9724 | N/A | 90.05 ± 6.53 | 93.76 ± 3.79 | N/A | N/A |
| Pang et al.[9] | FCM+Snake Algorithm | Semi-automatic | unknown [i] | 81.0 ± 10.0 | 0.968 [a, c] | N/A | 86.8 [b,c] | 90.9 [b,c] | 0.437 | N/A |
| Shi et al.[16] | FCM+Level Set | Automatic | 25 | Prechemo 81.0 ± 13.0/ Postchemo 71.0 ± 22.0 | N/A | N/A | N/A | N/A | Prechemo 0.918/ Postchemo 0.185 [e] | Prechemo 0.981/ Postchemo 0.994 [e] |
| Meinel et al.[31] | Connected Component | Semi-automatic | unknown [j] | 64.0 | N/A | N/A | N/A | N/A | N/A | N/A |

**Table 1.** Overview of the segmentation results

a Manual segmentation by an expert served as golden standard
b Diagnostic performance: calculated by the "leave-one-out cross validation" method
c Features: entropy, correlation, sum average, difference average and solidity
d Median of overlap
e Benign, fibroadenomas
f Malignant, non-triple negative*
g Malignant, triple negative*
h Testing is done on 10 synthetic images generated by random data
i Only number of benign and malignant breast lesions are reported, 22 and 38 respectively
j Only number of benign and malignant breast lesions are reported, 17 and 24 respectively

* Triple negative breast cancer is a molecular subtype that lacks expression of the estrogen, progesterone , and the HER2 receptors.

## III. Discussion

In this section, we review the segmentation methods for breast lesion that are presented above. It is important to mention that the datasets used for the evaluation of the methods are different from each other, what makes it hard to compare the segmentation results. Table 1 gives an overview of the results of the methods.

In Kannan et al. [15], most of the experiments are done on synthetic data, but results on the synthetic data was not directly comprehensible because the paper does not provide any explanation about how to interpret the data and the results. In Szabo et al. [25] and Lucht et al. [13] segmentation results are not evaluated quantitatively, instead the results are presented by the type of the lesion.

Cui et al. [7] employed a marker-controlled watershed transform to semi-automatically segment the lesions. In semi-automatic methods, in order to correctly segment the lesion and make it fast, it helps to first localize the lesion on the MRI image and select it with a rectangle. This can be either preferable in some cases resulting in a faster segmentation method but on the other hand this is not a segmentation method which is reproducible and robust at the same time.

*Fuzzy c-means (FCM)*

From the selection of key references, segmentation methods that are based on FCM are the most widely used approaches for breast lesion segmentation. FCM is used in several fields and in medical image segmentation. It is used for different purposes e.g. initial segmentation in Shi et al. [16]. In this study the initial segmentation, which is done by FCM clustering, is refined by level sets.

In Pang et al. [20], the FCM is also used to get an initial segmentation to use it to further refine it by applying the gradient vector flow (GVF) snake model. Also working with “internal” and “external” forces, the method performed such that the correlation increased in comparison with the radiologist manual segmentation without a significant difference at averages. This shows that by incorporating another method in combination with FCM improves segmentation results. Even so, the implementation of FCM in this report only uses the intensity information of the pixels whereas pharmacokinetic information, as done in Shi et al. [16], can be added as information and might improve it even further.

Kennan et al. [15] introduces a new objective function that replaces Euclidean distance measures for constructing an objective function. However, no evaluation metrics are used to present comparison results with the former algorithm. The modified algorithm is tested on a synthetic image generated by random data and on a real-life data of a breast MRI image, but it is not reported if the algorithm is tested on more real-life data.

In Chen et al. [14] they also used the FCM for the segmentation of breast lesions and compared it with a previous developed volume-growing (VG) method by Gilhuijs et al. [26]. The performance index that is used to come to this conclusion is based on the overlap measure (the intersection of $C$ and $R$ over the union of $C$ and $R$) given by

$$O = \frac{C \cap R}{C \cup R}$$

where $C$ is the set of voxels returned from the computerized segmentation and $R$ is the set of voxels in the radiologist's segmentation. A predetermined threshold is used to find out if the lesion is segmented correctly compared with the radiologist's segmentation. As can be seen in figure 2 this threshold is 0.4 and the number of correctly segmented lesion is based on this threshold. The study does not report why they have chosen 0.4 as the threshold and looking at the performance graph a different threshold can be chosen to get a higher number of correctly segmented lesions.

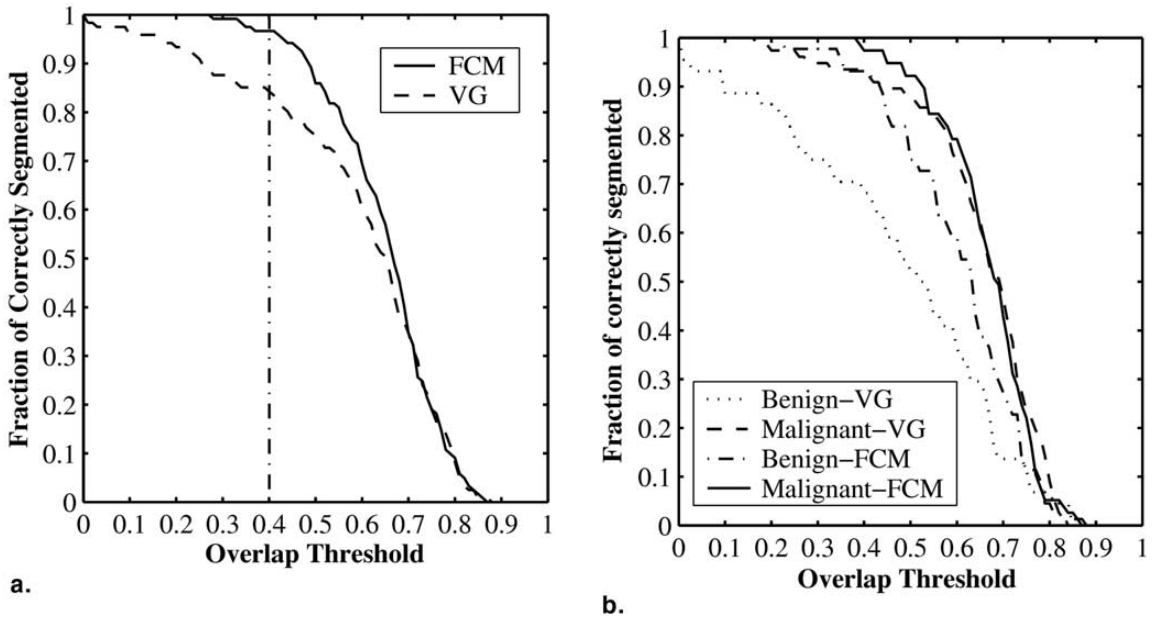


**Figure 2.** Performance of the proposed FCM-based lesion segmentation algorithm and VG algorithm on a clinical database of 121 mass lesions.

*Geodesic active contour*

In Shannon C et al. [22] lesions are segmented based on a geodesic active contour, the Magnetostatic Active Contour (MAC) model. From each of the 41 breast lesions the radiologist selected a lesion slice and analyses where done for that slice only. Although the study segments and detects lesions, the focus of the study was more to be able to distinguish between triple negative breast cancers from other types. Based on the example given of a segmentation the MAC segmentation corresponds well with the manual segmentation, but the evaluation given in this study is not comprehensive enough [Table 2], in my view, to give a critical opinion about the segmentation method used and it's results.

| *Lesion Type* | *HD* | *MAD* | *Sens.(%)* | *Spec.(%)* |
|---|---|---|---|---|
| Benign, FAs | 11.23 | 8.85 | 73 | 99 |
| Malignant, non-TN | 9.01 | 4.41 | 82 | 99 |
| Malignant, TN | 14.49 | 7.65 | 47 | 99 |

**Table 2.** Evaluation of Automated vs. Manual Segmentation.
HD-Hausdorff distance (voxels), MAD-Mean Absolute Distance (voxels), Sens-Sensitivity, Spec-Specificity

*Neural networks*

What is striking are the number of patient data that is used to test and evaluate the artificial neural networks. In Lucht et al. [13] and Szabó et al. [25] only 15 and 10 patient data are used, respectively. This is not a representative number of patient data to test a neural network. Neural networks need large sample data in order to get satisfactory approximation, theoretically [27]. And also the risk of over fitting is present [28].

In Zheng et al. [29] a comparison of the boundary distances is done between the computer-expert segmentation and the rough-expert segmentation where the mean and standard deviation are 4.10-5.62 pixels and 7.67-8.24 pixels respectively. This comparison eventually will give a better score because the segmentation compared with is rough only and therefore a refinement will be better logically [Figure 3]. For the evaluation of the performance of the segmentation algorithm only a ROC curve is given. For a better understanding of the performance of the developed graph cut based segmentation, more evaluation methods should have been used and presented.

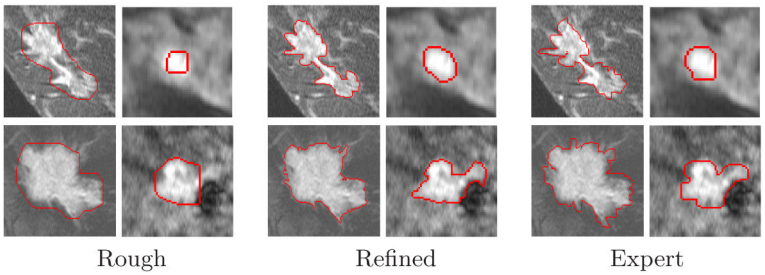


**Figure 3.** Rough manual segmentations by a manual rater, corresponding refined results, and manual segmentations by an expert

Woods et al.[30] presents a method to distinguish between nonmalignant and malignant tissues with the use of four-dimensional (4D) co-occurrence-based texture analysis. The report does not present a concrete method to segment the lesions automatically, but instead two radiologists manually segment the lesions. These manual segmentation were used in a model-free neural network-based classification system that assigned each voxel a “nonmalignant” or “malignant” label. Based on these labels a segmentation could also be done.

The segmentation method in Schlossbauer et al.[31] was done automatically by marking pixels for segmentation if the initial signal increase was at least 50%. Next the lesion in question was extracted with a region growing algorithm, where a voxel within each lesion is selected by only 1

observer by a mouse-click. Because of the risk that the lesion segmentation will suffer from interobserver-variability, a analyses was done in a sample of 20 lesions. Although a high correlation was found ($R^2 = 0.98$), the number of samples is too low compared with the 85 focal lesions that were analyzed.

| | N | Precision error |
|---|---|---|
| Manual | 30 | 4.89% |
| Robust Computer | 30 | 0.89% |

**Table 3.** Robustness of the ROI selection

*Connected Component*

Notable was the fact that the datasets used in this study were acquired from different imaging protocols and at different institutions. Consequently, this shows how robust the developed algorithm is and may help to improve it in future research.

In order to work with the differences in the data, some preprocessing steps are required. Rather than working on the data that takes the entire time-intensity curve into account, the algorithm works on a subtraction image that is used by the radiologist to visually assess the lesion morphology. The reason behind this choice is that the time-intensity curve would make the algorithm more prone to errors resulting from motion artifacts. But these motion artifacts could be corrected by registration methods.

Although the study showed that the ROI selection using the seed-point selection is more robust than the manual method [Table 3], it was only tested on breast lesions that were mass-like. In order for the algorithm to work on non-mass-like lesions as well, a modification of the algorithm is required.

Segmentation methods that make use of user interaction are called semi-automatic methods. In semi-automatic methods, a user helps in finding the location of the tumor in the breast and defines a region of interest or places a seed point. Pang et al. [9] employed a semi-automatic method in which a rectangle ROI is defined. This way the search area of the method is restricted to the given localization making the segmentation accuracy higher. On the other hand, it takes some time for the user to locate the tumor and define a ROI or placing a seed point. Furthermore, the localization done by the user can suffer from inter- and intraobserver variability i.e. the user can localize a bigger or smaller ROI or place the seed at a different location the next time. Therefore, the initial result is sensitive to the selection of the ROI or the placement of a seed point and may result in a less robust semi-automatic method. To prevent this variability and obtaining a result faster, a fully automatic method can be used instead, but the accuracy would be lower compared to semi-automatic methods.

In either way, regardless of the segmentation method, it is very important to segment the whole lesion without missing any parts. Necrotic areas in the tumor can complicate this because the necrotic parts do not get any contrast agent because of dead tissue concentration and therefore

they might have low contrast. Because of this low enhancement this part could be partitioned as nonlesion and cause “holes” in the segmentation, e.g. in a FCM procedure. Meinel et al. [10] and Chen et al. [14] dealt with this problem by applying a hole-filling operation in their post-processing part of the segmentation process in order to include the necrotic area into the segmentation result.

But even with no necrotic area present in the tumor, incorrect segmentation can occur due to low contrast between tumour and surrounding tissue. It is difficult to correctly segment breast lesions in low contrast images because the border is hardly visible. By administering a contrast agent, the contrast in the image is improved, making it easier to distinguish the tumour from the surrounding tissue. Because in semi-automatic methods human interaction is involved, the user takes time to locate the tumour. Additionally, the user defines a region of interest that is given as input to the method and therefore already delimiting the search area for borders of the lesion. However, in fully automatic methods no human interaction is involved making it difficult for the method to produce a good segmentation in low contrast images. Still, in order to get good results some preprocessing needs to be done on the image. In the marker-controlled watershed method [30], smoothing is applied on the image to deal with low contrast images. But on the other hand, because it is dependent on a gradient image it may lead to oversegmentation.

The same is true with segmentation of lesions that are irregular in shape. There will be oversegmentation with methods that are based on intensity values e.g. FCM and region growing. But since these methods don’t care about shapes but only on pixel intensities they are, nevertheless, able to segment a lesion that is irregular in shape. Other methods e.g. geodesic active contour will perform better than FCM and region growing because curvature information is included in the formula. However, in the case of a lesion with spikes (very high curvature), the active contour algorithms may have problems in getting enough force to drive the contour toward the boundary [35]. Table 4 shows the ability of each method dealing with specific problems. These specific problems are related to either the state of the whole image or the lesion itself that has to be segmented. But structures that somewhat resemble lesions are also a problem that can easily occur in fully automatic methods since no user interaction is involved. Blood vessels also have high intensities on contrast-enhanced MR images and can therefore falsely be recognized by the method as a lesion. Patient motion, especially around the edge of the breast, can also include that area in the segmentation process. Chen et al. [34] performs a 3D connected-component labeling operation on the binary ROI to reduce confusing structures. There is no further information on how the other fully automatic methods would deal with confusing structures. What may be possible is to apply some post-processing to remove confusing structures based on texture or, in most cases of malignant lesions, on border attributes i.e. if the border has the attributes of a spiculated contour or irregular shape.

The articles use different datasets for testing what makes it difficult to compare the results of the different methods and not all articles report a sensitivity and specificity. The articles that do report these evaluation criteria, all report high specificity. Specificity is defined as the ability to identify negative results written as:

$$\text{specificity} = \frac{\text{number of true negatives}}{\text{number of true negatives} + \text{number of false positives}}$$

The specificity are all high mostly because the area covered by the tumour in the region of interest is relatively small compared to the background making the number of true negatives big, resulting in a high specificity. As for the low sensitivity of lesion type malignant triple negative in Shannon et al. [24], it may have to do with the specific attributes of a triple negative lesion that are not included yet in the segmentation method since the non triple negative lesion has a more plausible sensitivity. In clinical practice, the high specificity reported in the articles may be to optimistic. The low sensitivity of triple negative lesions on the other hand may a problem since it will not be usable in clinical practice before improving the sensitivity.

More challenges and bottlenecks exist before we are able to use fully automatic segmentation of breast lesions in DCE-MRI in clinical practice. Further research has to be done in order to tackle challenges such as the difficulty of segmentation in low contrast images. Improving this area may lead to a smaller dose of contrast agent. Other challenges are to avoid structures that somewhat resemble lesions, producing good results in images with intensity inhomogeneity and noise. Finally, a bottleneck may be the missing of a central dataset that can be used to evaluate the methods with. This way, the different methods can easily be compared.

| Segmentation method | Low contrast? | Irregularly shaped lesion? |
|---|---|---|
| Cui et al.[30] Marker-controlled watershed | Yes | No |
| Shannon et al.[24] Geodesic Active Contour | No | Yes |
| Woods et al.[28] Neural Network | Yes | No |
| Schlossbauer et al.[29] Region growing | Yes | Yes |
| Zheng et al.[27] Graph-Cut | No | No |
| Chen et al.[34] FCM | No | Yes |
| Szabó et al.[21] Neural Network | Yes | No |
| Lucht et al.[14] Neural Network | Yes | No |
| Kannan et al.[15] FCM | No | Yes |
| Azmi et al.[22] New MRF | No | Yes |
| Pang et al.[9] FCM+Snake Algorithm | No | Yes |
| Shi et al.[16] FCM+Level Set | Yes | Yes |
| Meinel et al.[31] Connected Component | No | Yes |

**Table 4.** Ability of methods to deal with specific problems

## IV. Conclusion

The purpose of this review was to give an overview of the different methods that exist for breast lesion segmentation in DCE-MRI. In this collection of methods, semi-automatic and full-automatic methods were discussed. Every method that is presented in this review is able to segment breast lesions in DCE-MRI images.

Segmentation in DCE-MRI images has substantial diagnostic power, such that it has potential to assist physicians in the assessment of volume changes. The enhancement of the lesions on the images make DCE-MRI a valuable technique for better segmentation of breast lesions.

The lack of large datasets in most studies, makes it necessary that research groups need closer cooperation. This allows for a larger study population, which can provide more valuable research results. Combining more than one method would increase the performance of segmentation as in Pang et al. [20] where the initial segmentation is done with FCM and refined with a level set. Based on the results in each article, the algorithm in Pang et al. [20] shows good results. This way of segmenting breast lesions in DCE-MRI images may not be fast, but good and robust results may be achieved. In that sense, further studies could be to combine different methods to achieve fast results as well.

## References (key references are in bold)


1. Lehman, Constance D., et al. "MRI evaluation of the contralateral breast in women with recently diagnosed breast cancer." *New England Journal of Medicine* 356.13 (2007): 1295-1303.
2. Shute, Nancy. "Beyond Mammograms." *Scientific American* 304.5 (2011): 32-34.
3. Eliat, Pierre-Antoine, et al. "Magnetic resonance imaging contrast-enhanced relaxometry of breast tumors: an MRI multicenter investigation concerning 100 patients." *Magnetic resonance imaging* 22.4 (2004): 475-481.
4. Boetes, Carla, et al. "Breast tumors: comparative accuracy of MR imaging relative to mammography and US for demonstrating extent." *Radiology* 197.3 (1995): 743-747.
5. Esserman, Laura, et al. "Utility of magnetic resonance imaging in the management of breast cancer: evidence for improved preoperative staging."*Journal of Clinical Oncology* 17.1 (1999): 110-110.
6. Malur, Sabine, et al. "Comparison of written reports of mammography, sonography and magnetic resonance mammography for preoperative evaluation of breast lesions, with special emphasis on magnetic resonance mammography." *Breast Cancer Research* 3.1 (2000): 55.
7. **Cui, Yunfeng et al. "Malignant lesion segmentation in contrast-enhanced breast MR images based on the marker-controlled watershed." *Medical physics* 36 (2009): 4359.**
8. Vincent, Luc. "Morphological grayscale reconstruction in image analysis: Applications and efficient algorithms." *Image Processing, IEEE Transactions on* 2.2 (1993): 176-201.
9. Yan, Jiayong, et al. "Marker-controlled watershed for lymphoma segmentation in sequential CT images." *Medical physics* 33 (2006): 2452.
10. **Meinel, Lina A et al. "Robust segmentation of mass−lesions in contrast−enhanced dynamic breast MR images." *Journal of Magnetic Resonance Imaging* 32.1 (2010): 110-119.**
11. Brix, Gunnar et al. "Microcirculation and microvasculature in breast tumors: pharmacokinetic analysis of dynamic MR image series." *Magnetic Resonance in Medicine* 52.2 (2004): 420-429.
12. Taylor, June S et al. "MR imaging of tumor microcirculation: promise for the new millenium." *Journal of Magnetic Resonance Imaging* 10.6 (1999): 903-907.
13. **Lucht, Robert, Stefan Delorme, and Gunnar Brix. "Neural network-based segmentation of dynamic MR mammographic images." *Magnetic resonance imaging* 20.2 (2002): 147-154.**
14. **Chen, Weijie, Maryellen L Giger, and Ulrich Bick. "A Fuzzy C-Means (FCM)-Based Approach for Computerized Segmentation of Breast Lesions in Dynamic Contrast-Enhanced MR Images< sup> 1</sup>." *Academic radiology* 13.1 (2006): 63-72.**
15. **Kannan, SR et al. "Robust kernel FCM in segmentation of breast medical images." *Expert Systems with Applications* 38.4 (2011): 4382-4389.**

**16. Shi, Jiazheng et al. "Treatment response assessment of breast masses on dynamic contrast-enhanced magnetic resonance scans using fuzzy c-means clustering and level set segmentation." *Medical physics* 36 (2009): 5052.**

17. Shi, Jiazheng, et al. "Characterization of mammographic masses based on level set segmentation with new image features and patient information."*Medical physics* 35 (2008): 280.

18. Osher, Stanley, and Ronald Fedkiw. *Level set methods and dynamic implicit surfaces*. Vol. 153. Springer, 2003.

19. Suri, Jasjit S., et al. "Shape recovery algorithms using level sets in 2-D/3-D medical imagery: a state-of-the-art review." *Information Technology in Biomedicine, IEEE Transactions on* 6.1 (2002): 8-28.

**20. Pang, Yachun et al. "Computerized segmentation and characterization of breast lesions in dynamic contrast-enhanced mr images using fuzzy c-means clustering and snake algorithm." *Computational and mathematical methods in medicine* 2012 (2012).**

**21. Azmi, Reza, and Narges Norozi. "A new markov random field segmentation method for breast lesion segmentation in MR images." *Journal of medical signals and sensors* 1.3 (2011): 156.**

**22. Agner, Shannon C et al. "Segmentation and classification of triple negative breast cancers using DCE-MRI." *Biomedical Imaging: From Nano to Macro, 2009. ISBI'09. IEEE International Symposium on* 28 Jun. 2009: 1227-1230.**

23. Xie, Xianghua, and Majid Mirmehdi. "MAC: Magnetostatic active contour model." *Pattern Analysis and Machine Intelligence, IEEE Transactions on* 30.4 (2008): 632-646.

24. Boykov, Yuri, Olga Veksler, and Ramin Zabih. "Fast approximate energy minimization via graph cuts." *Pattern Analysis and Machine Intelligence, IEEE Transactions on* 23.11 (2001): 1222-1239.

**25. Szabó, Botond K, Peter Aspelin, and Maria Kristoffersen Wiberg. "Neural network approach to the segmentation and classification of dynamic magnetic resonance images of the breast: Comparison with empiric and quantitative kinetic parameters< sup> 1</ sup>." *Academic radiology* 11.12 (2004): 1344-1354.**

26. Gilhuijs, Kenneth GA, Maryellen L Giger, and Ulrich Bick. "Computerized analysis of breast lesions in three dimensions using dynamic magnetic-resonance imaging." *Medical physics* 25 (1998): 1647.

27. Zhang, Guoqiang Peter. "Neural networks for classification: a survey." *Systems, Man, and Cybernetics, Part C: Applications and Reviews, IEEE Transactions on* 30.4 (2000): 451-462.

28. Lawrence, Steve, and C Lee Giles. "Overfitting and neural networks: Conjugate gradient and backpropagation." *Neural Networks, 2000. IJCNN 2000, Proceedings of the IEEE-INNS-ENNS International Joint Conference on* 2000: 114-119.

**29. Zheng, Yuanjie et al. "Segmentation and classification of breast tumor using dynamic contrast-enhanced MR images." *Medical Image Computing and Computer-Assisted Intervention–MICCAI 2007* (2007): 393-401.**

**30. Woods, Brent J et al. "Malignant−lesion segmentation using 4D co−occurrence texture analysis applied to dynamic contrast−enhanced magnetic resonance breast image data." *Journal of Magnetic Resonance Imaging* 25.3 (2007): 495-501.**

**31. Schlossbauer, Thomas et al. "Classification of small contrast enhancing breast lesions in dynamic magnetic resonance imaging using a combination of morphological criteria and dynamic analysis based on unsupervised vector-quantization." *Investigative radiology* 43.1 (2008): 56.**

**32. Rominger, Marga B et al. "Accuracy of MRI volume measurements of breast lesions: comparison between automated, semiautomated and manual assessment." *European radiology* 19.5 (2009): 1097-1107.**

**33. Lucas−Quesada, Flora Ann, Usha Sinha, and Shantanu Sinha. "Segmentation strategies for breast tumors from dynamic MR images." *Journal of Magnetic Resonance Imaging* 6.5 (1996): 753-763.**

34. Soille, Pierre. "Morphological Image Processing: Principles and Applications." (1999).

35. Davatzikos, Christos, and Jerry L. Prince. "Convexity analysis of active contour problems." *Image and vision computing* 17.1 (1999): 27-36.